Medical Engineering and Physics 91 (2021) 1–11

Contents lists available at ScienceDirect

Medical Engineering and Physics

journal homepage: www.elsevier.com/locate/medengphy

# Modelling the leptomeningeal collateral circulation during acute ischaemic stroke

Raymond M. Padmos[a,*], Nerea Arrarte Terreros[b,c], Tamás I. Józsa[d], Gábor Závodszky[a], Henk A. Marquering[b,c], Charles B.L.M. Majoie[b], Alfons G. Hoekstra[a]

[a] Computational Science Laboratory, Informatics Institute, Faculty of Science, University of Amsterdam, Science Park 904, Amsterdam 1098 XH, the Netherlands
[b] Department of Radiology and Nuclear Medicine, Amsterdam UMC, location AMC, Amsterdam, the Netherlands
[c] Department of Biomedical Engineering and Physics, Amsterdam UMC, location AMC, Amsterdam, the Netherlands
[d] Institute of Biomedical Engineering, Department of Engineering Science, University of Oxford, Parks Road, Oxford OX1 3PJ, UK

ARTICLE INFO

*Article history:*
Received 24 November 2020
Revised 26 February 2021
Accepted 10 March 2021

*Keywords:*
Acute ischaemic stroke
Leptomeningeal collateral circulation
1D blood flow model
Cerebral contrast transport
Collateral flow simulation

ABSTRACT

A novel model of the leptomeningeal collateral circulation is created by combining data from multiple sources with statistical scaling laws. The extent of the collateral circulation is varied by defining a collateral vessel probability. Blood flow and pressure are simulated using a one-dimensional steady state blood flow model. The leptomeningeal collateral vessels provide significant flow during a stroke. The pressure drop over an occlusion predicted by the model ranges between 60 and 85 mmHg depending on the extent of the collateral circulation. The linear transport of contrast material was simulated in the circulatory network. The time delay of peak contrast over an occlusion is 3.3 s in the model, and 2.1 s (IQR 0.8–4.0 s) when measured in dynamic CTA data of acute ischaemic stroke patients. Modelling the leptomeningeal collateral circulation could lead to better estimates of infarct volume and patient outcome.



## 1. Introduction

The cerebral collateral circulation consists of alternative pathways that provide blood flow when the primary circulation is blocked [1]. These alternative pathways are critical for patient outcome during and after an acute ischaemic stroke (AIS). Brain tissue death occurs in the order of a few minutes in the absence of flow, while treatment times are typically in the order of several hours [2]. If brain tissue is to survive till treatment, blood flow has to be sustained. The collateral circulation ensures sustained blood flow to brain tissue during an AIS, reducing cell death and brain tissue injury. The extent of collateral flow is highly variable among patients [3]. Poor collateral flow is associated with worse outcome after AIS [4]. Collateral flow is one of the most significant predictors of patient outcome [4–7].

The primary collateral circulatory system of the brain is the circle of Willis (CoW). The CoW sits at the start of the cerebral circulation and interconnects the starting branches of the major cerebral arteries. Various configurations of the CoW exist, with about half the population having a complete circle [8]. The secondary collateral circulatory system includes the leptomeningeal collateral vessels, and is the focus of this article. The leptomeningeal collateral vessels are small with a diameter below 1 mm, and generally below the resolution of most imaging systems [9–11]. These vessels sit at the pial surface and interconnect various branches of the major cerebral arteries (middle, anterior, and posterior) [9].

Quantitative data on the leptomeningeal collateral vessels in humans are lacking. Most experimental data on these vessels come from animal experiments [12–14]. Their existence is often disputed or thought to be too small to provide any significant flow [9]. In addition, these vessels are believed to only become active during a major event such as AIS [15]. Collateral flow can be observed during an AIS and the existence of the collateral vessels inferred. Predicting penumbra and infarct volumes, and patient outcome after stroke requires the assessment of the extent of collateral flow [16,17]. Models of the cerebral circulation generally include multiple configurations of the CoW [18–20]. However, the secondary collateral vessels are often excluded.

We present a computational model of the leptomeningeal collateral circulation. This model is an extension of our previous model [21,22]. The circulatory system is created using a combination of (literature) data and statistical scaling laws. We include an explicit representation of the pial surface network including the

* Corresponding author.
*E-mail address:* r.m.padmos@uva.nl (R.M. Padmos).

https://doi.org/10.1016/j.medengphy.2021.03.003

leptomeningeal collateral circulation to capture collateral flow after stroke onset. The extent of the leptomeningeal collateral circulation can be varied by a single parameter defined as the collateral vessel probability.

Blood flow and pressure are simulated using a one-dimensional (1D) steady state blood flow model. Contrast transport through the circulation is also simulated, relying on an upwind finite-difference model for linear advection. We compare our model with dynamic computed tomography angiography (CTA) measurements performed in AIS patients. The model is able to reproduce the measurements in stroke patients. We show that the leptomeningeal collateral vessels are able to provide significant flow during AIS. Simulating the effect of stroke on brain tissue thus requires the inclusion of the leptomeningeal collateral circulation.

## 2. Methods

### 2.1. Generation of the circulatory network

The network presented here builds upon our previous model [21,22], shown in Fig. 1a and b. In short, the vasculature starts at the heart and includes the vessels between the heart and the CoW. The cerebral vessels at the CoW are extended with the major cerebral vessels, taking from a publicly available data set, the BraVa data set [23]. A vessel segmentation is randomly chosen to be added to the network from the data set. The brain mesh was postprocessed using a publicly available model [24,25]. Superficial perfusion territories have been identified based on vascular atlases obtained from arterial spin labelling perfusion MRI as described in [26–28]. Different configurations of the CoW can be included by removing vessels from the complete circle. The complete circle is used here. The circulatory network is then expanded by adding bifurcating trees, that perfuse dedicated brain perfusion areas. To this earlier published model, the pial network including the leptomeningeal collateral vessels is added, as well as penetrating arteries that act as model outlets.

Each cerebral vessel outlet is mapped to the pial surface and assumed to have its own perfusion territory. These territories are determined by our mapping algorithm previously published [22]. A bifurcating tree is generated at each cerebral vessel outlet, see Fig. 1c, using Murray's law and a length-radius ratio of 10 [29]. Murray's law is given by $R_i^3 = r_i^3 + r_j^3$ where $R$ denotes the mother branch and $r$ the daughter branches. A symmetric bifurcating tree is generated until the daughter vessels reach a cut-off radius of 200 µm. The mapping algorithm assigns surface area on the pial surface to the outlets of the large cerebral vessels, as shown in Fig. 1b [22]. The area assigned to the outlet is perfused by the bifurcating tree connected to the outlet. The outlets of the bifurcating tree are assumed to have their own perfusion territory within the area assigned to the entire tree.

One constraint is that outlets that connect to the same mother vessel have connected perfusion territories on the surface. This can be achieved by iteratively dividing the surface in two, as we move downstream of the bifurcating tree to the outlets, see Fig. 1d. The division algorithm uses Metis (a graph partitioning library) to divide the subgraphs in two equally sized connected regions [30]. Finally, the node that has the smallest maximum distance to the other nodes (minimal eccentricity) of the subgraph is taken to be the centre of the region, and connects the outlet of the bifurcating tree to the pial vessel network.

Little is known about the pial vessel network in humans. Most studies are done on rats or mice [12–14]. However, assuming the vasculature of rats and mice is similar to that of humans, the pial network can be approximated by a hexagonal mesh or honeycomb mesh [31]. The density of the hexagons or loops is not known for humans. In measurements of mice and rats, the loop area is about 1 mm$^2$ [31]. However, the density of penetrating arteries also differs between species, 1.0/mm$^2$ in human, 7.9/mm$^2$ in monkey, 8.3/mm$^2$ in rats and 3.9/mm$^2$ in mice [32]. A larger loop size seems appropriate given the difference in penetrating artery density, otherwise the density of these loops and the penetrating arteries would be equal. In the model, the area of each loop is roughly 5 mm$^2$.

The pial network is generated by taking the dual graph of the pial surface (defined as a triangulation). The dual graph of a triangulation is a hexagonal mesh. The size and number of the loops in the pial network can be set by remeshing the pial surface to a uniform triangulation with a set number of triangles. The model contains about 20,000 loops, see Fig. 1e and f. The outlets of the bifurcating trees are connected to the nearest node of the pial network. Penetrating arteries are generated uniformly on the surface of the brain with a density of 1.0 per mm$^2$ [32]. The penetrating arteries connect to the nearest node of the pial network. The diameter of the pial network vessels, including those to the penetrating arteries outlets, are set to 400 µm. The diameter measured in human cadavers ranges from 200 to 610 µm for arteries of the cerebrum and 180 to 543 µm for the arteries of the cerebellum [11].

A collateral vessel is defined as a vessel that crosses perfusion domains on the pial surface as determined by our mapping algorithm [22]. The leptomeningeal collateral circulation is part of the pial network previously generated, see Fig. 1f. A collateral vessel probability is used to determine whether a collateral vessel is included in the circulatory network. This probability is defined as the chance that a vessel is included in the circulatory network. Every leptomeningeal collateral vessel, i.e. the red vessels shown in Fig. 1e and f, has a chance to be included in the pial network depending only on the collateral vessel probability.

### 2.2. *Steady state blood flow modelling*

Blood vessels are modelled as thin elastic tubes and blood as an incompressible viscous fluid. Every vessel segment is modelled as a resistance. The equations are derived from those used in 1D blood flow modelling with the added assumption that the velocity derivatives in time and space are zero. The pressure in the network is calculated by solving the mass-balance equation given by

$$\sum_j G_{ij}\left(P_i - P_j\right) = S_i \tag{1}$$

with $G_{ij}$, the conductance in m$^3$/Pa s (inverse of resistance) between nodes $i$ and $j$, and $S_i$ a source term for every node $i$. The conductance of a segment is given by $G = \pi r^4/2(\zeta + 2)\mu L$, where $r$ is the radius, $L$ is the segment length, $\mu$ is the dynamic viscosity set to 3.5 mPa s, and $\zeta$ is a unitless constant related to the velocity profile, with 2 representing a parabolic profile, i.e. laminar flow, and 9 representing a flatter profile used in this model [33]. The larger constant is the result of a blunt velocity profile in the vessels [34]. It is not exactly known how the velocity profiles changes throughout the circulation. A blunt profile is still a good description in arterioles [35].

The resulting equations can be written as a linear system given by

$$G\vec{\boldsymbol{P}} = \begin{bmatrix} \sum^{G_{1j}} & -G_{12} & \cdots & -G_{1N} \\ -G_{21} & \sum^{G_{2j}} & \cdots & -G_{2N} \\ \vdots & \vdots & \ddots & \vdots \\ -G_{N1} & \cdots & \cdots & \sum^{G_{Nj}} \end{bmatrix} \begin{bmatrix} P_i \\ \vdots \\ \vdots \\ P_N \end{bmatrix} = \begin{bmatrix} S_i \\ \vdots \\ \vdots \\ S_N \end{bmatrix} = \vec{\boldsymbol{S}} \tag{2}$$

Flow rate boundary conditions can be set by assigning a non-zero value to the source term vector. Pressure boundary conditions can be set by assigning pressure values to the source term vector and updating the rows of the conductance matrix to have a value

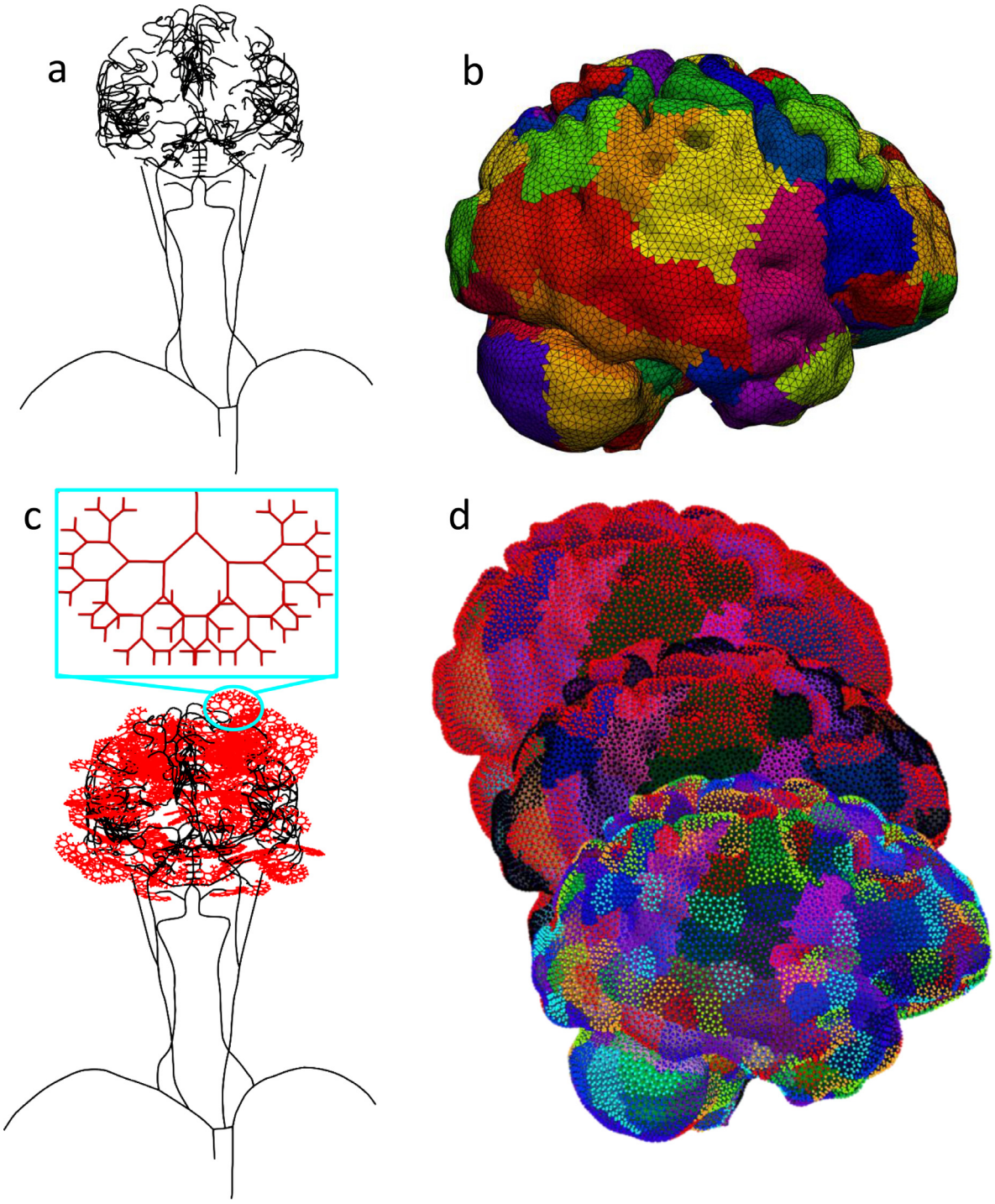


**Fig. 1.** (**a**) The large arteries used in the model, starting at the heart and ending at the major cerebral arteries. (**b**) The surface mapping on the surface of the brain. Each colour denotes the perfusion territory of a single outlet of the large arteries in (a). Shown is the right side of the brain. (**c**) At the outlets of the large cerebral arteries in (a), a bifurcating tree is generated. (**d**) The bifurcating trees are mapped on the surface by iterative division of the perfusion territories in (b). Shown is the right side of the brain. (**e**) The pial vessel network model of the brain. Shown is the bottom side of the brain. Vessels are shown in black with the leptomeningeal collateral vessels in red. (**f**) Close up view on the pial surface in (d). Each polygon represents one penetrating artery outlet with the colours indicating different major cerebral regions. (For interpretation of the references to color in this figure legend, the reader is referred to the web version of this article.)

of one on the diagonal and zero elsewhere. This system is solved by lower-upper (LU) decomposition. The radius of each vessel node is updated based on a pressure-area relationship that described the elastic response of the vessel [36]. The pressure-area relationship is given by

$$P = P_0 + \frac{\sqrt{\pi}Eh}{A_0\left(1-\nu^2\right)}\left(\sqrt{A} - \sqrt{A_0}\right) \tag{3}$$

where $A$ is the cross-sectional area, $A_0$ is the initial area, $P$ is the pressure, $P_0$ is a reference pressure set to the diastolic pressure, $E$ is the Young's modulus, $h$ is the wall thickness and $\nu$ is the Poisson ratio of the vessel wall set to ½. The values for the large systemic arteries (i.e. from the ascending aorta to the CoW) can be found in Padmos et al., 2021 [22]. The Young's modulus for all cerebral vessels is set to 1.6 MPa.

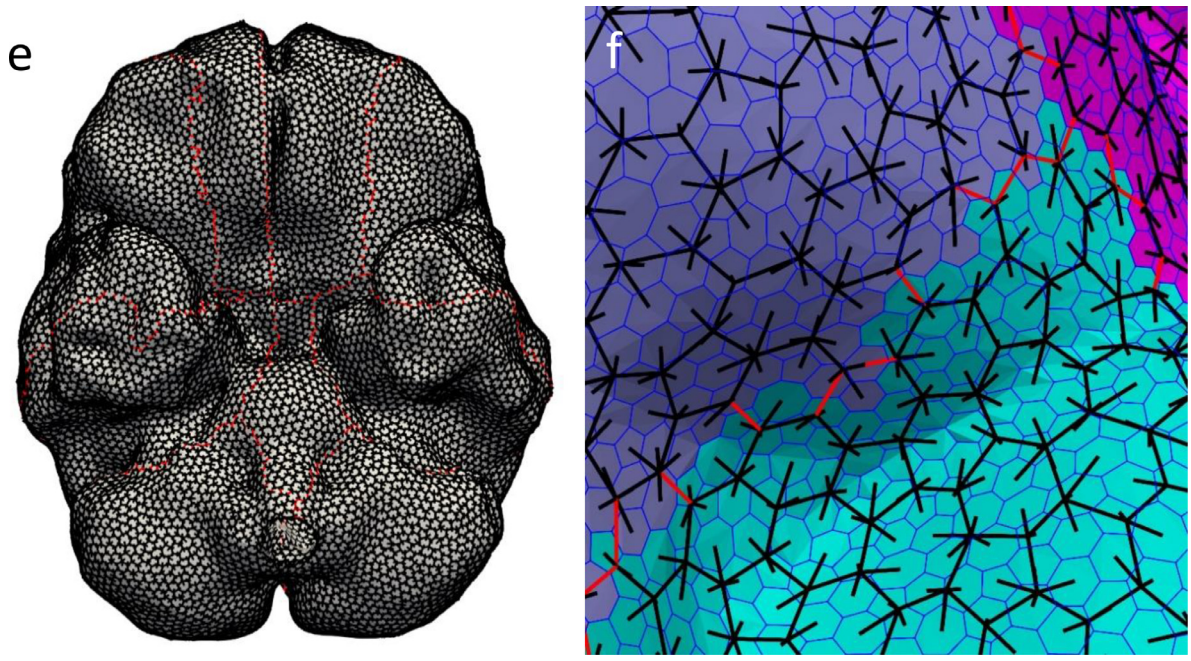


**Fig. 1.** Continued

The conductance matrix $G$ is updated based on the new radii. The system is solved iteratively until a pressure tolerance, $\varepsilon_P$, of $10^{-6}$ is reached defined as

$$\varepsilon_P = \frac{\left|\vec{\boldsymbol{P_i}} - \overrightarrow{\boldsymbol{P_{i-1}}}\right|}{\left|\vec{\boldsymbol{P_i}}\right|} \tag{4}$$

with $\vec{\boldsymbol{P_i}}$ and $\overrightarrow{\boldsymbol{P_{i-1}}}$ being the pressure vectors during the i-th and (i-1)-th iterations, respectively. Every vessel is discretised with a minimum of three nodes and a maximum number of nodes set by a maximum segment length of 2.5 mm between nodes. An AIS is modelled as the complete blockage of a vessel by setting the conductance $G$ in segments containing an occlusion to zero.

The volume flow rate in a segment, $Q_{ij}$, is calculated as

$$Q_{ij} = \frac{\left(P_i - P_j\right)}{R_{ij}}, \tag{5}$$

where $R_{ij}$ is the resistance of the segment. The velocity, $v_{ij}$, is calculated as

$$v_{ij} = \frac{Q_{ij}}{\pi\left(0.5r_i + 0.5r_j\right)^2}, \tag{6}$$

where $r$ is the radius of the vessel nodes.

At the start of the ascending aorta, a volumetric flow rate is set based on stroke volume and heart rate: $Q_{in} = SV^*HR/60$ and is set to 70 mL/s (SV = 70, HR = 60). At the outlets, a resistance is used that captures the pressure drop between the outlet and the right atrium. The pressure at the right atrium is set to $P_{out}$ = 666 Pa ≈ 5 mmHg.

The resistance of the total network (before autoregulation, see below) is calculated as $R_T = dp/Q_{in}$ with $dp$, the pressure drop over the heart determined by subtracting the mean right atrial pressure from the mean arterial pressure. Mean arterial pressure is calculated as $1/3^*P_{sys} + 2/3^*P_{dia}$, where $P_{sys}$ is the systolic and $P_{dia}$ is the diastolic pressure [37]. $P_{sys}$ *and* $P_{dia}$ are 17.5 kPa and 10.0 kPa respectively, resulting in a mean arterial pressure of 12.5 kPa.

Most of the vasculature, such as the limbs, organs, etc., is not included in the model, and we have to account for this with appropriate boundary conditions. The resistance at the outlets of the large systemic vessels is distributed based on their cardiac output fraction. The cardiac output fraction of the large systemic outlets are 0.75, 0.05, and 0.05 for the Thoracic aorta, R. Brachial, and L. Brachial respectively [38]. The outlet resistance is determined as $R = R_T/CO_f$ with $CO_f$ the cardiac output fraction. The rest of the resistance is distributed to the external carotid arteries and cerebral vessels. If there are multiple outlets for a specific region, the resistances are distributed based on the fraction of cubic radii [22].

At the outlets on the pial surface, the resistance is adjusted to capture the effect of autoregulation. The resistance of every penetrating artery outlet is calculated to achieve a desired volumetric flow rate. The resistance is updated according to

$$R = \frac{(P_i - P_{out})}{(Q_{brain} \;/\; N_{pa})} \tag{7}$$

There are limits to the range of autoregulation. The outlet resistance is limited by

$$R_{low} = \frac{P_{low}}{(Q_{brain} \;/\; N_{pa})}, R_{upp} = \frac{P_{upp}}{(Q_{brain} \;/\; N_{pa})} \tag{8}$$

where $P_{low}$ and $P_{upp}$ set the pressure limits at which the penetrating artery can no longer regulate flow. The outlet resistance is limited between the lower and upper bounds. $P_{low}$, $P_{upp}$, *and* $Q_{brain}$ are set to 10 mmHg, 100 mmHg, and 12.5 mL/s, respectively [39,40].

The steady state model is solved again with the updated resistance. This is iterated until a flow rate tolerance of $10^{-6}$ is reached defined as

$$\varepsilon_Q = \frac{\left|\vec{\boldsymbol{Q_i}} - \overrightarrow{\boldsymbol{Q_{i-1}}}\right|}{\left|\vec{\boldsymbol{Q_i}}\right|} \tag{9}$$

with $\vec{\boldsymbol{Q_i}}$ being the flow rate vector during the i-th iteration and $\overrightarrow{\boldsymbol{Q_{i-1}}}$ being the flow rate vector from the (i-1)-th iteration.

### 2.3. Contrast advection modelling

Contrast transport is simulated as advection dominant flow of an incompressible fluid. The 1D advection equation, assuming constant area and velocity within the vessel, is given by

$$\frac{\partial C}{\partial t} + v_x \frac{\partial C}{\partial x} = 0. \tag{10}$$

At merger points, such as bifurcations, the contrast concentration is a sum of the relative volume flowing into the system, given by

$$C_{out} = \frac{\sum^{C_i} Q_i}{\sum^{Q_i}} = \sum^{C_i} f_i \tag{11}$$

where the summation runs over connected nodes with flow directed towards that merger point. That is, the contrast concentration out of a merger point assumes uniform mixing of contrast flowing into the merger point. The $C_i$ *and* $Q_i$ are obtained by solving the 1D advection Equation, Eq. (10), and steady state blood flow, Eq. (5), respectively.

A first-order finite-difference upwind scheme is used to discretize the Equation. The resulting system of linear equations is written in matrix notation as

$$\begin{bmatrix} C_1^{t+\Delta t} \\ \vdots \\ \vdots \\ \vdots \\ C_N^{t+\Delta t} \end{bmatrix} = \boldsymbol{B} \begin{bmatrix} 1 & 0 & 0 & \cdots \\ v_x\Delta t/\Delta x & 1 - v_x\Delta t/\Delta x & 0 & \ddots \\ 0 & v_x\Delta t/\Delta x & 1 - v_x\Delta t/\Delta x & 0 \\ \vdots & \ddots & \ddots & \ddots \\ 0 & \cdots & 0 & v_x\Delta t/\Delta x \end{bmatrix} \begin{bmatrix} 0 \\ \vdots \\ \vdots \\ \vdots \\ 1 - v_x\Delta t/\Delta x \end{bmatrix} \begin{bmatrix} C_1^t \\ \vdots \\ \vdots \\ \vdots \\ C_1^t \end{bmatrix} \tag{12}$$

where $\boldsymbol{B}$ is a merging point matrix with elements $B_{ij} = f_j$ if flow at node i is directed away from the merger point and flow at node j is directed towards the same merger point, otherwise $B_{ii} = 1$ and $B_{ij} = 0$.

Contrast transport over time is calculated by iterative matrix multiplication. At the inlet vessel, i.e. the heart, a short segment is added such that the next time step can be calculated only by matrix multiplication. Alternatively, the contrast vector at time t can be updated at every time step. A bolus of contrast injected into the system is modelled as a sharp Gaussian function (arbitrary units) with height 10 and variance 125. The function is shifted such that the peak appears at the inlet after 1 s. Contrast transport is simulated for 40 s. The time delay in peak contrast over the occlusion is calculated as the time difference in peak contrast between the merger points at the proximal and distal ends of the blocked vessel, see Fig. 2c and d.

### 2.4. Time delay over an occlusion measured in AIS patients

The time delay over the occlusion is the time blood spends travelling from the beginning to the end of the occlusion. These times are measured in dynamic CTA data of 49 AIS patients from the Amsterdam University Medical centre and the Dutch acute stroke trial (DUST) [41]. These patients had a single large vessel occlusion in the middle cerebral artery (MCA). From the dynamic CTA data, contrast arrival along the occluded vessel is observed by measuring the time attenuation curves. The time delay between the beginning and the end of the occlusion is computed using cross-correlation.

## 3. Results

### 3.1. Circulatory network

The various parts of the model are shown in Fig. 1. The model includes the large arteries starting at the heart, the CoW, the major cerebral branches, the smaller cerebral vessels as bifurcating trees, the pial network vessels including the leptomeningeal collateral vessels and the vessels leading to the penetrating arteries. The network contains around 600,000 nodes, and 187,000 vessels (the exact number depends on the number of collateral vessels).

The red coloured vessels in Fig. 1e and f show the location of variability of the collateral circulation in the model. The variability is set by assigning a collateral vessel probability between the major cerebral regions, i.e. cerebellum, brain stem, and left and right middle, anterior and posterior regions. The collateral vessel probability independently determines for each collateral vessel (i.e. the red coloured vessels in Fig. 1e and f) if it is included in the network.

### 3.2. Blood flow and contrast transport modelling

Blood flow velocity and pressure are simulated using a 1D steady state blood flow model and contrast advection is simulated using a linear advection model, see Fig. 2. Fig. 3 shows the flow rate to the penetrating arteries during a stroke for various collateral vessel probabilities. The occlusion is located in the right MCA. Generation of the network, the blood flow simulation and the contrast advection takes approximately 20, 10 and 10 min, respectively per simulation on an AMD Ryzen 7 3700X 8-core processor (3.60 GHz) with 16 GB RAM. The blood flow simulations typically converge within ten iterations.

Injection of a contrast bolus into the venous system is simulated as starting from the heart. Fig. 4, shows the time of peak contrast arrival on the pial surface and Fig. 5 shows the pressure drop over the occlusion and time delays in peak contrast over the occlusion for various collateral vessel probabilities. The time delays in the model reaches a minimum of 3.3 s. The median time delay measured on dynamic CTA data of AIS patients is 2.1 s (IQR 0.8 s–4.0 s). The pressure drop over the occlusion in the model ranges between 60 and 85 mmHg and decreases as the collateral vessel probability increases.

### 3.3. Measurements in AIS patients

Fig. 6 shows the measurements of the contrast time delays over the occlusion in AIS patients. Table 1 lists the measured and modelled results for the time delays and pressure drop over the occlusion. The simulation results are in satisfactory agreement with clinical time delay and pressure drop measurements.

## 4. Discussion

Constructing a model of the leptomeningeal collateral circulation requires combining data from multiple sources. The complete

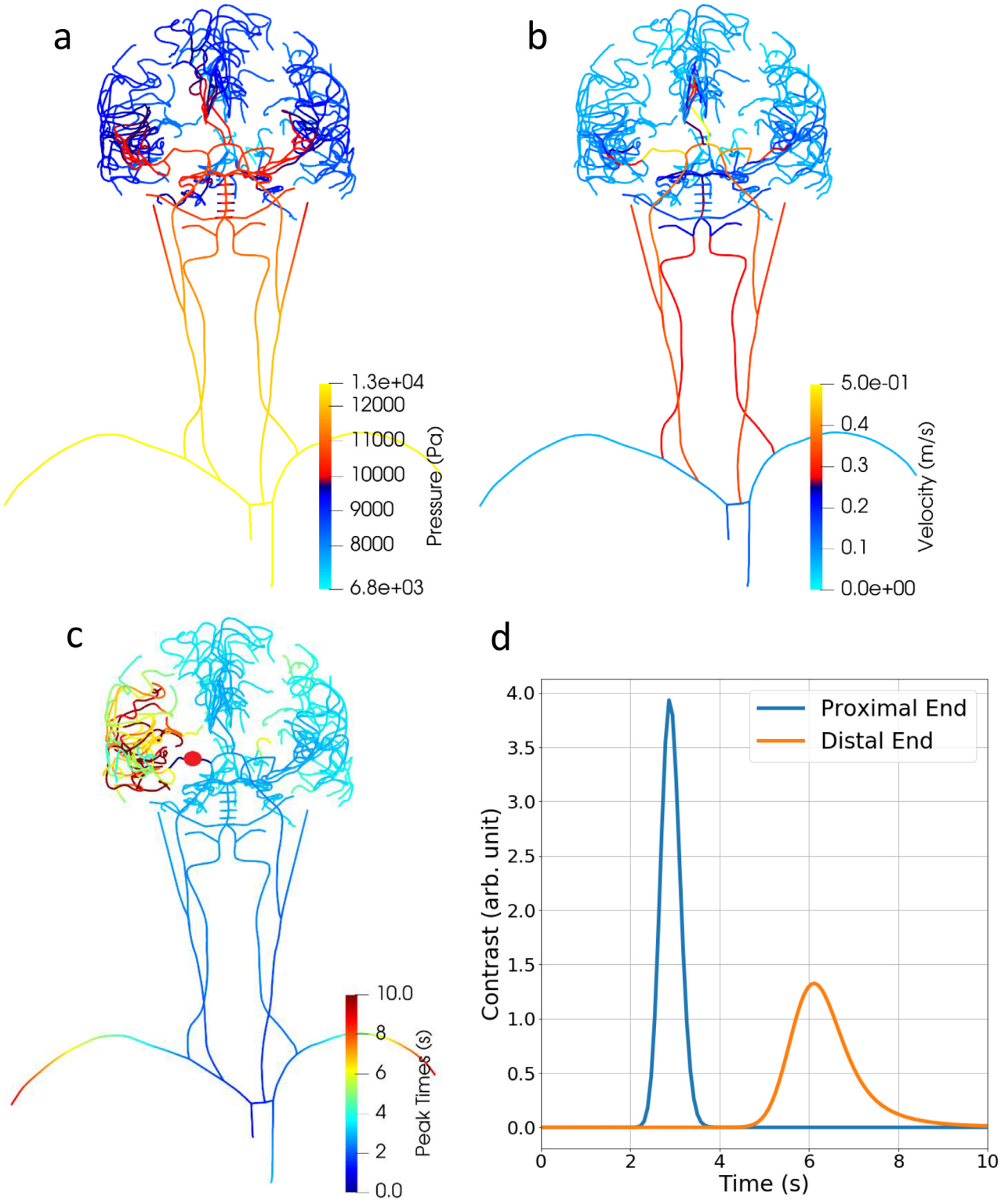


**Fig. 2.** Results from the steady state blood flow model and contrast advection model in the large systemic arteries to the cerebral arteries. (a) Blood pressure for a healthy patient. (b) Blood flow velocity for a healthy patient. (c) Arrival time of peak contrast during a stroke. The occlusion is located in the right MCA as indicated by the red dot. The simulated network has a collateral probability of one. (d) Contrast profiles over time at the proximal and distal ends of the vessel, i.e. right MCA, containing an occlusion. (For interpretation of the references to color in this figure legend, the reader is referred to the web version of this article.)

vessel network, shown in Fig. 1, includes the large arteries to the brain, the large cerebral arteries, the smaller cerebral arteries that connect to the pial network, the pial network and the penetrating arteries as the outlets. The leptomeningeal collateral vessels are part of the pial network.

The pial network vessels connect to the penetrating arteries that penetrate the white and grey matter of the brain [44]. The outlets of the model at the pial surface do not penetrate the surface. There are two reasons for this. Firstly, the penetrating arteries can be regarded as perfusing their own independent tissue col-

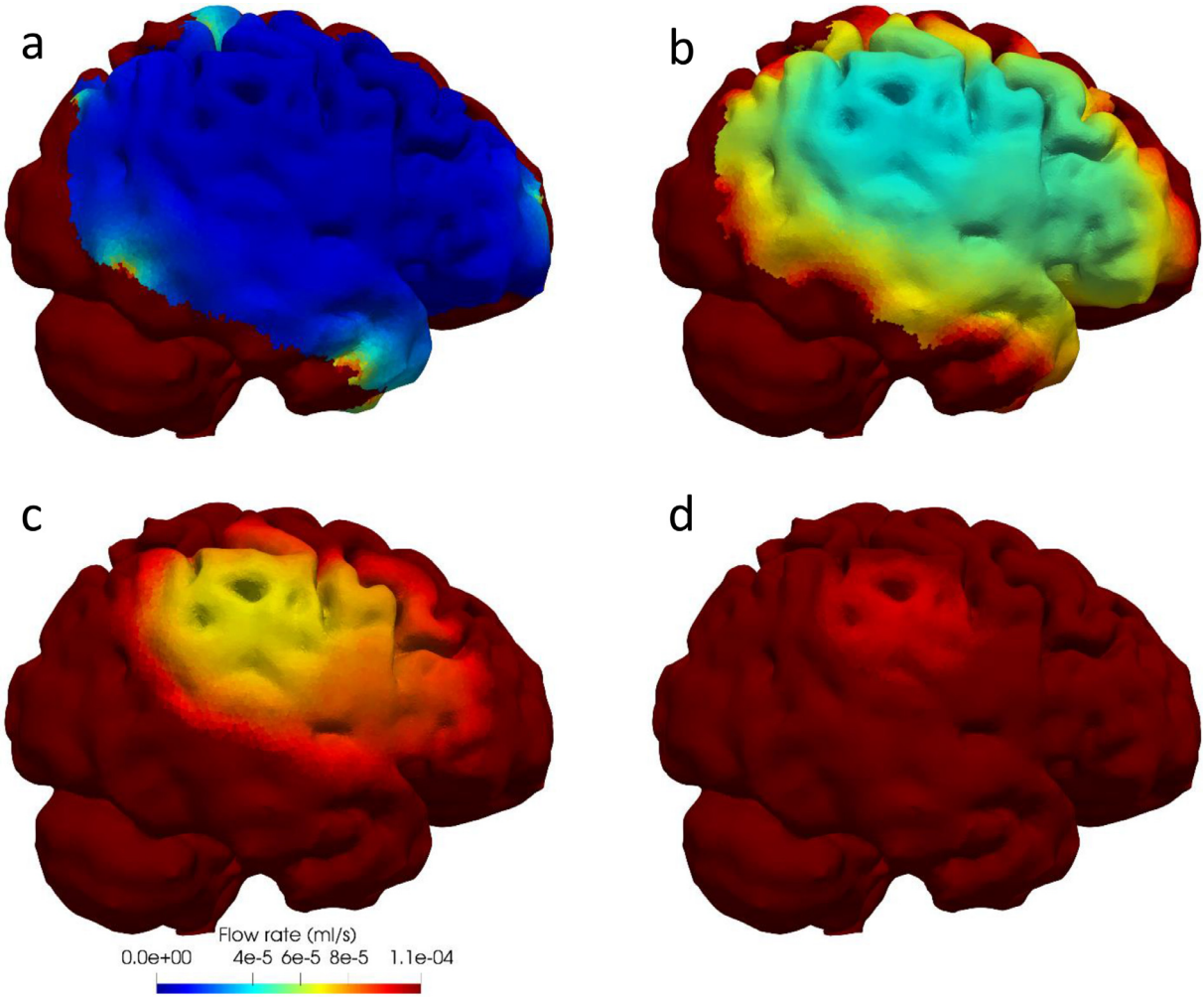


**Fig. 3.** Flow rate at the penetrating artery outlets on the pial surface. Shown is the right side of the brain with the region affected by an occlusion in the right MCA. The collateral vessel probabilities are (a) 0.01, (b) 0.10, (c) 0.40 and (d) 1.0 in order from left to right. (For interpretation of the references to color in this figure legend, the reader is referred to the web version of this article.)

**Table 1**
Measured vs modelled values.

| Variable Name: | Measured Value: | Simulated Value: |
|---|---|---|
| Time delay over the occlusion [s] | 2.1 (0.8 - 4.0) median (IQR) [41]<br>1.3 (0.1 – 3.7) median (IQR) (Anterograde flow)<br>3.8 (1.5 – 6.5) median (IQR) (Retrograde flow) [42] | 3.3 |
| Pressure drop over the occlusion [mmHg] | 56.7 ± 18.0 (mean ± SD, mRS of 0–2),<br>63.1 ± 19.1 (mean ± SD, mRS of 3–6) [43] | 60 - 85 |

SD: Standard deviation, IQR: interquartile range, mRs: modified Rankin scale.

umn (although there is some overlap between neighbours) and we can regard each outlet as a unit of tissue [45]. Secondly, simulating the entire microcirculation of the brain as individual vessels is very demanding and computationally expensive. In addition, the cellular nature of blood becomes increasingly important and requires a different model. In the future, the model presented here will be extended with a continuous tissue model for the micro circulation [21]. Our final aim is to create a model that is able to provide an estimate of the infarct volume after a stroke. Our proposed model for the leptomeningeal collateral circulation will be a very relevant feature of this overall model. When looking at the leptomeningeal collateral circulation, the microcirculation and venous circulation do not have to be explicitly simulated if proper boundary conditions are used.

An alternative approach by Phan et al. [46], is to model the leptomeningeal collaterals as connections between the major cerebral vessels. However, this can lead to overestimation of their size as there is likely not a direct (single) connection between the vessels. Instead, the leptomeningeal collaterals likely function through multiple parallel pathways for collateral flow. In addition, we aim to create a model that is able to provide an estimate of the infarct volume after an AIS. The model therefore has to include the vessels to the white and grey matter of the brain.

The results should be interpreted within the limits of the model. Firstly, the model is created from data of different sources and patients. As a result, the circulatory network does not belong to, and likely differs significantly from, any real patient. However, we believe that the general findings will not differ significantly. We aim to show that the leptomeningeal collateral circulation can explain at least some of the variability in collateral flow observed between AIS patients. Secondly, many of the model parameters are assumed to be constant to keep the model tractable. Lastly, the generated vessels are not optimised to achieve uniform pressure on the surface. A zero-pressure gradient at the pial surface could explain why the leptomeningeal collateral vessels appear to be dormant in healthy patients. These limitations could be overcome by

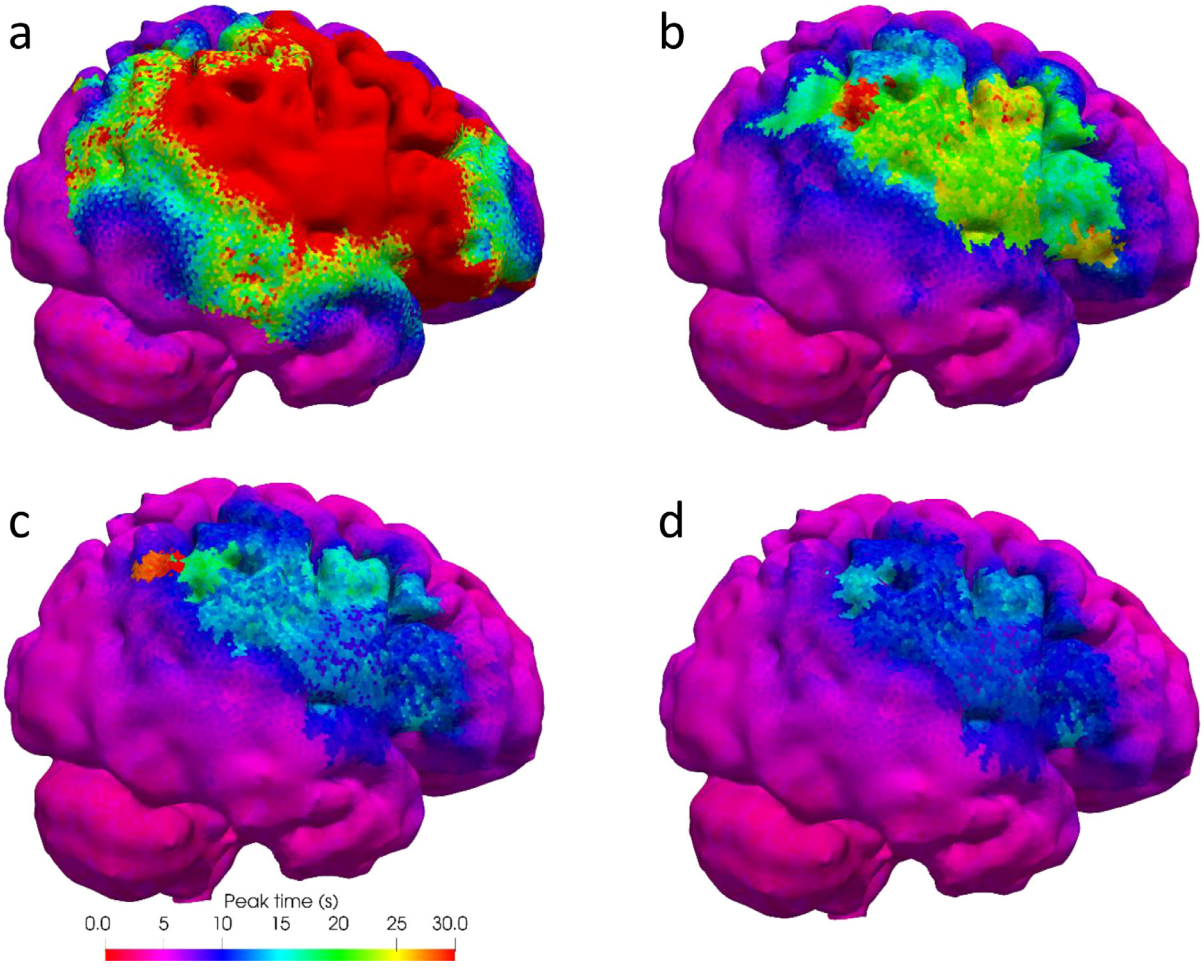


**Fig. 4.** Arrival time of peak contrast at the penetrating arteries on the pial surface. Shown is the right side of the brain with the region affected by an occlusion in the right MCA. The collateral vessel probabilities are (a) 0.01, (b) 0.10, (c) 0.40 and (d) 1.0 in order from left to right. (For interpretation of the references to color in this figure legend, the reader is referred to the web version of this article.)

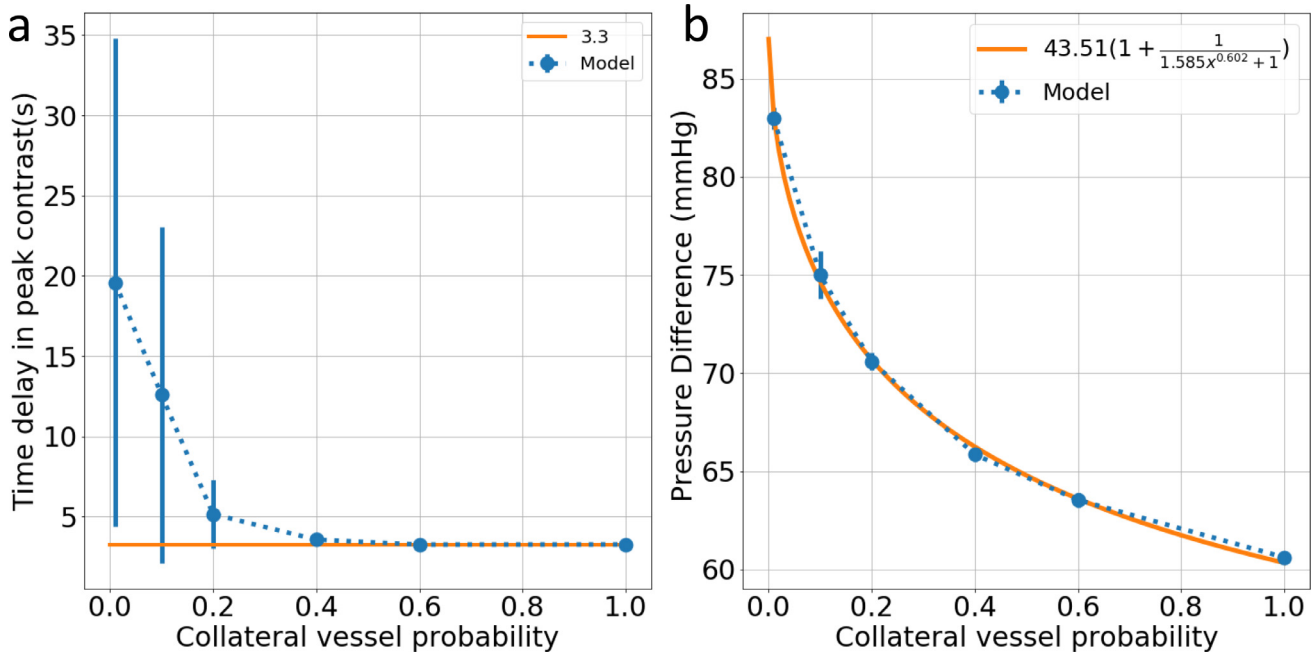


**Fig. 5.** (a) Time delay in peak contrast over the occlusion as a function of the collateral vessel probability. The error bars show the standard deviation over five simulations. The orange line shows minimal time delay in the model. (b) Pressure drop over the occlusion as a function of the collateral vessel probability. The error bars show the standard deviation over five simulations. The orange line shows a fit to a power law based on multiple parallel resistances. (For interpretation of the references to color in this figure legend, the reader is referred to the web version of this article.)

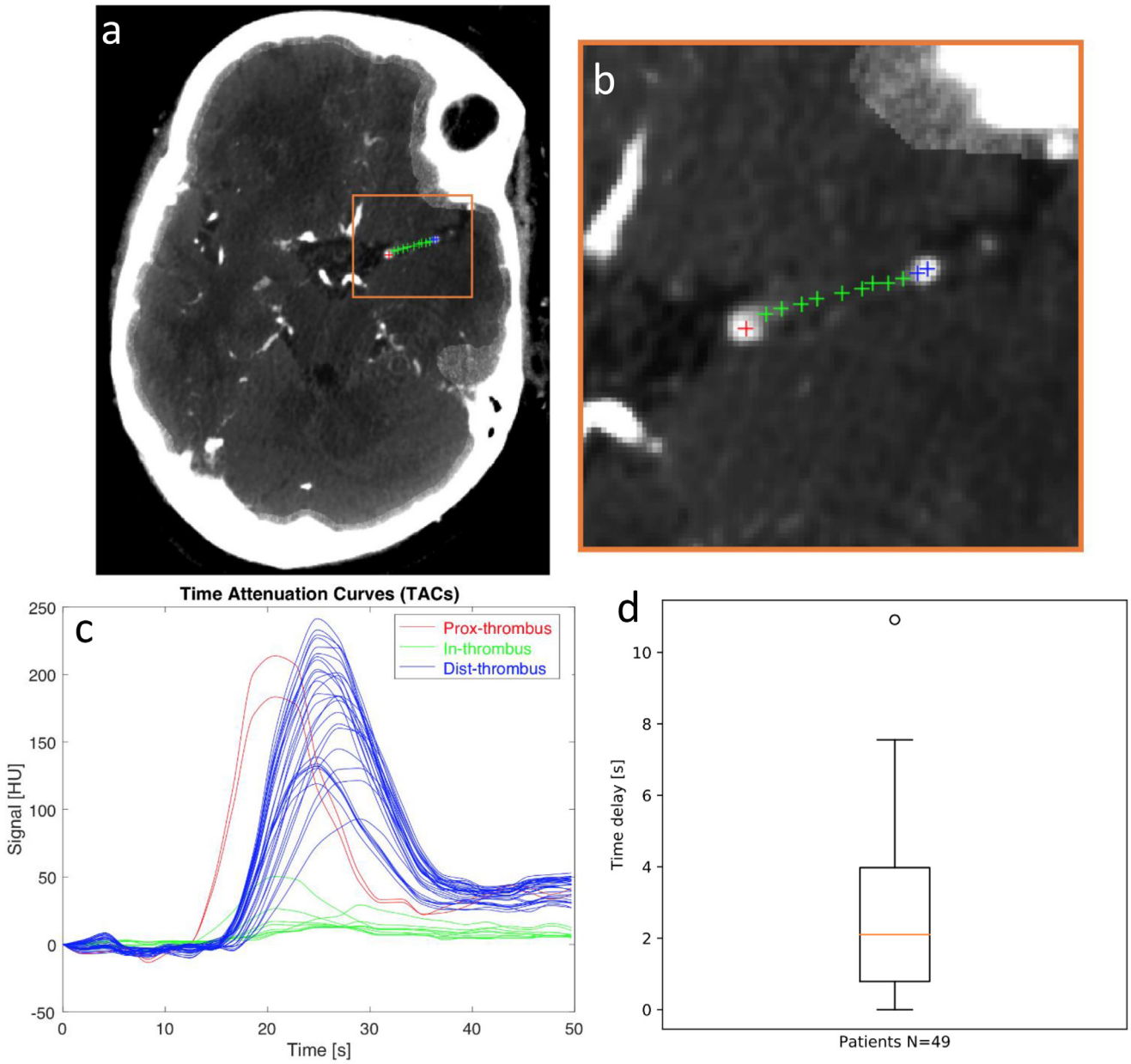


**Fig. 6.** (**a**) Example of a dynamic CTA scan of an AIS patient with a left MCA occlusion. Markers are placed proximal, in, and distal to the thrombus in red, green, and blue, respectively. (**b**) Close-up of the region selected in (a) showing the occlusion location and the placed markers. (**c**) Example of time attenuation curves in Hounsfield units extracted from the placed markers. Each line shows the time attenuation curve of a single placed marker. (**d**) Boxplot of the performed measurements for 49 AIS patients. (For interpretation of the references to color in this figure legend, the reader is referred to the web version of this article.)

creating high-resolution data sets including the correlations of all relevant parameters.

Blood flow through the vasculature is modelled using a steady state approach, see Fig. 2. The steady state approach is chosen for its simplicity and more importantly, the time scale of interest, i.e. tissue infarction, which is much longer than the cardiac cycle. All simulated strokes are right MCA strokes as these are the most common type of large vessel occlusions [2]. Fig. 3 shows the flow rate at the pial surface during an AIS. Variation of the leptomeningeal collateral circulation causes large differences in pressure and flow rate at the pial surface during a stroke. Increasing the number of collateral vessels increases blood flow to the affected region. Better collateral flow is a result of higher throughput through the collateral vessels to the affected tissue.

Cerebral autoregulation is the process by which the brain is able to maintain constant blood flow by vessel dilation and constriction [47,48]. This is an important effect that the model should capture. Cerebral autoregulation in this model ensures uniform flow rates to the brain in the healthy scenario. The assumption is that we are in the valid pressure range for autoregulation. The resistance of every penetrating artery outlet is set to achieve a desired flow rate. The resistance is limited to an upper and lower bound: at high pressures, the vessel is maximally constricted; at low pressure, the vessel is maximally dilated. The pressure used to define the resistance limits are defined at the entrance of the penetrating artery. Therefore, these values are lower than the arterial pressure normally reported for autoregulation limits [47,49].

As brain tissue dies, pericytes die off, which causes vessels to constrict [50]. This increases the resistance to flow of the penetrat-

ing arteries and causes flow to decrease. This effect is not included in the model. The simulation therefore only represents the brain at the instantaneous moment of a vessel occlusion, i.e. stroke onset. Over time, the resistance at the penetrating arteries (model outlets) is expected to increase due to pericyte death, resulting in decreased flow and growth of the infarct core. The collateral vessels affect the growth of the infarct core by allowing tissue to survive longer. The collateral vessels are small, i.e. 200 µm in the model, with relative high resistance with respect to the large arteries. The path of least resistance in the model, during a stroke, is therefore that of retrograde flow through the large vessels of the major cerebral arteries. If the thrombus is permeable or only partially occluding the vessel, the path of least resistance can be through the (partially) occluded vessel, resulting in anterograde flow.

Fig. 4 shows the time of peak contrast arrival on the pial surface. Having better collateral circulation decreases the arrival time of peak contrast across the pial surface. The magnitude of peak arrival time is similar to those measured by CT perfusion imaging [51]. Fig. 5 shows the effect of increasing the collateral vessel probability on the time delay and pressure drop over the occlusion. The time delay in the model ranges between 19.6 and 3.3 s, and depends on the extent of the collateral circulation. The time delay decays exponentially towards a minimum of 3.3 s. Note that a collateral vessel probability of zero will result in an infinite delay. The contrast time delay over the occlusion observed in AIS patients, see Fig. 6, is between 0.8 and 4.0 s (interquartile range) with a median of 2.1 s. The time delays in the model are of the same order of magnitude as measured in AIS patients.

The pressure drop over the occlusion decreases as the collateral vessel probability increases. One explanation for the found relationship is that the addition of collateral vessels results in additional pathways to the network, similar to adding parallel resistances to an electrical circuit. The orange line in Fig. 5 shows a fitted curve of similar form as that for resistors in parallel. Note that in this circulatory network, the resistances are not equal and the equation is changed to a power law. The pressure drop over the occlusion ranges between 60 and 85 mmHg in the model. The pressure drop over the occlusion measured in AIS patients varies between 56.7 ± 18.0 mmHg and 63.1 ± 19.1 mmHg (mean±SD) depending on the modified Rankin scale [43]. The model is able to reproduce a pressure drop in this range.

The thrombus is simulated as a complete blockage of flow and pressure; a real thrombus could result in a partial occlusion of the vessel. These partial occlusions can lead to anterograde flow through the thrombus. Anterograde flow results in a lower time delay of 1.3 s (IQR 0.1 s–3.7 s) versus 3.8 s (IQR 1.5 s–6.5 s) [42]. Note that these values include different occlusion locations. Table 1 shows an overview of the measurements in AIS patients and values derived from the model. Whether the flow through a permeable thrombus or partial occlusion is able to significantly affect infarct volume is not known.

A lower collateral vessel probability results in increased variance in the time delay, as shown by the increased standard deviation in Fig. 5a. The location and number of leptomeningeal collateral vessels determine the velocity and flow patterns of collateral flow. As the collateral vessel probability decreases, the effect of spatial variation of the collateral vessels becomes significant. The pressure at the distal end of the occlusion also varies more, but as the collateral vessel probability decreases, the pressure at the proximal end becomes dominant. As the collateral vessel probability decreases, the time delay becomes infinite while the pressure at the distal end approaches the venous pressure.

AIS patients likely vary significantly in the extent of their collateral circulation. Moreover, there are likely other pathways that contribute to the measured time delay and pressure drop over the occlusion that are not present in the model. Patient-specific parameters, such as vessel radii, Young's modules, diastolic and systolic blood pressures, etc., will affect the observed time delay and pressure drop over the occlusion. The extent of the collateral circulation could be estimated in AIS patients, e.g. by measuring the pressure drop over the occlusion, for inclusion in predictive models. As the leptomeningeal collateral circulation is responsible for significant flow to affected regions, it should be included in models of stroke.

## 5. Conclusion

A blood flow model with contrast transport of the cerebral circulation including the leptomeningeal collateral vessels is proposed. Variability of the collateral circulation leads to variability in collateral flow to tissue at risk during an acute ischaemic stroke. The model is able to capture this variability in collateral flow including the effect of retrograde flow. The time delay and pressure drop over an occlusion predicted by the model match those measured in AIS patients. The leptomeningeal collateral circulation plays an important role in predictions of infarct volume and patient outcome, and should be included in models of stroke and the cerebral circulation.

## Declaration of Competing Interest

Charles Majoie: Related: Grant from European Commission; Unrelated: Grants from CVON/Dutch Heart Foundation, Stryker, TWIN Foundation, Health Evaluation Netherlands (all paid to institution); shareholder of Nico-lab, a company that focuses on the use of artificial intelligence for medical image analysis (modest). The other authors declare that there is no conflict of interest.

## Funding

This project (INSIST; www.insist-h2020.eu) has received funding from the European Union's Horizon 2020 research and innovation programme under grant agreement No 777072.

## Ethical approval

Data collection was approved by the ethical review boards of the participating medical centres. All patients or legal representatives gave informed consent to use their data, conforming to the European Union General Data Protection Regulation.

## Authors' Contributions

R.M. Padmos wrote the manuscript and developed the computational model. N. Arrarte Terreros performed the measurements in stroke patients. T.I. Józsa has postprocessed the brain mesh and the vessel-encoded arterial spin labelling MRI atlas describing perfusion territories. G. Závodszky, H.A. Marquering, C.B.L.M. Majoie and A.G. Hoekstra helped conceive and supervise the project. All authors have contributed to the final manuscript.

## References

[1] Liebeskind DS. Collateral circulation. Stroke 2003;34:2279–84. doi:10.1161/01.STR.0000086465.41263.06.
[2] Berkhemer OA, Fransen PSS, Beumer D, van den Berg LA, Lingsma HF, Yoo AJ, et al. A randomized trial of intraarterial treatment for acute ischemic stroke. N Engl J Med 2015;372:11–20. doi:10.1056/NEJMoa1411587.
[3] Kim JJ, Fischbein NJ, Lu Y, Pham D, Dillon WP. Regional angiographic grading system for collateral flow. Stroke 2004;35:1340–4. doi:10.1161/01.STR.0000126043.83777.3a.
[4] Kimmel ER, Al Kasab S, Harvey JB, Bathla G, Ortega-Gutierrez S, Toth G, et al. Absence of collaterals is associated with larger infarct volume and worse outcome in patients with large vessel occlusion and mild symptoms. J Stroke Cerebrovasc Dis 2019:1–6. doi:10.1016/j.jstrokecerebrovasdis.2019.03.032.

[5] Jung S, Wiest R, Gralla J, Mckinley R, Mattle H, Liebeskind D. Relevance of the cerebral collateral circulation in ischaemic stroke: time is brain, but collaterals set the pace. Swiss Med Wkly 2017;147:1–28. doi:10.4414/smw.2017.14538.
[6] Vagal A, Aviv R, Sucharew H, Reddy M, Hou Q, Michel P, et al. Collateral clock is more important than time clock for tissue fate. Stroke 2018;49:2102–7. doi:10.1161/STROKEAHA.118.021484.
[7] Seners P, Roca P, Legrand L, Turc G, Cottier JP, Cho T-H, et al. Better collaterals are independently associated with post-thrombolysis recanalization before thrombectomy. Stroke 2019;50:867–72. doi:10.1161/STROKEAHA.118.022815.
[8] Papantchev V, Stoinova V, Aleksandrov A, Todorova-Papantcheva D, Hristov S, Petkov D, et al. The role of willis circle variations during unilateral selective cerebral perfusion: a study of 500 circles. Eur J CardioThorac Surg 2013;44:743–53. doi:10.1093/ejcts/ezt103.
[9] Brozici M, van der Zwan A, Hillen B. Anatomy and functionality of leptomeningeal anastomoses: a review. Stroke 2003;34:2750–62. doi:10.1161/01.STR.0000095791.85737.65.
[10] Malhotra K, Liebeskind DS. Collaterals in ischemic stroke. Brain Hemorrhages 2020;1:6–12. doi:10.1016/j.hest.2019.12.003.
[11] Vander Eecken HM, Adams RD. The anatomy and functional significance of the meningeal arterial anastomoses of the human brain. J Neuropathol Exp Neurol 1953;12:132–57. doi:10.1097/00005072-195304000-00002.
[12] Stromberg DD, Fox JR. Pressures in the pial arterial microcirculation of the cat during changes in systemic arterial blood pressure. Circ Res 1972;31:229–39. doi:10.1161/01.RES.31.2.229.
[13] Armitage GA, Todd KG, Shuaib A, Winship IR. Laser speckle contrast imaging of collateral blood flow during acute ischemic stroke. J Cereb Blood Flow Metab 2010;30:1432–6. doi:10.1038/jcbfm.2010.73.
[14] Chalothorn D, Clayton JA, Zhang H, Pomp D, Faber JE. Collateral density, remodeling, and VEGF-A expression differ widely between mouse strains. Physiol Genom. 2007;30:179–91. doi:10.1152/physiolgenomics.00047.2007.
[15] Tariq N, Khatri R. Leptomeningeal collaterals in acute ischemic stroke. J Vasc Interv Neurol 2008;1:91–5.
[16] Seyman E, Shaim H, Shenhar-Tsarfaty S, Jonash-Kimchi T, Bornstein NM, Hallevi H. The collateral circulation determines cortical infarct volume in anterior circulation ischemic stroke. BMC Neurol 2016;16:206. doi:10.1186/s12883-016-0722-0.
[17] Lima FO, Furie KL, Silva GS, Lev MH, Camargo ECS, Singhal AB, et al. The pattern of leptomeningeal collaterals on CT angiography is a strong predictor of long-term functional outcome in stroke patients with large vessel intracranial occlusion. Stroke 2010;41:2316–22. doi:10.1161/STROKEAHA.110.592303.
[18] Alastruey J, Parker KH, Peiró J, Byrd SM, Sherwin SJ. Modelling the circle of Willis to assess the effects of anatomical variations and occlusions on cerebral flows. J Biomech 2007;40:1794–805. doi:10.1016/j.jbiomech.2006.07.008.
[19] McConnell FK, Payne S. The dual role of cerebral autoregulation and collateral flow in the circle of willis after major vessel occlusion. IEEE Trans Biomed Eng 2017;64:1793–802. doi:10.1109/TBME.2016.2623710.
[20] Safaei S, Blanco PJ, Müller LO, Hellevik LR, Hunter PJ. Bond graph model of cerebral circulation: toward clinically feasible systemic blood flow simulations. Front Physiol 2018;9:1–15. doi:10.3389/fphys.2018.00148.
[21] Józsa TI, Padmos RM, Samuels N, El-Bouri WK, Hoekstra AG, Payne SJ. A porous circulation model of the human brain for in silico clinical trials in ischaemic stroke. Interface Focus 2021;11:20190127. doi:10.1098/rsfs.2019.0127.
[22] Padmos RM, Józsa TI, El-Bouri WK, Konduri PR, Payne SJ, Hoekstra AG. Coupling one-dimensional arterial blood flow to three-dimensional tissue perfusion models for in silico trials of acute ischaemic stroke. Interface Focus 2021;11:20190125. doi:10.1098/rsfs.2019.0125.
[23] Wright SN, Kochunov P, Mut F, Bergamino M, Brown KM, Mazziotta JC, et al. Digital reconstruction and morphometric analysis of human brain arterial vasculature from magnetic resonance angiography. Neuroimage 2013;82:170–81. doi:10.1016/j.neuroimage.2013.05.089.
[24] Garcia-Gonzalez D, Race NS, Voets NL, Jenkins DR, Sotiropoulos SN, Acosta G, et al. Cognition based bTBI mechanistic criteria; a tool for preventive and therapeutic innovations. Sci Rep 2018;8:10273. doi:10.1038/s41598-018-28271-7.
[25] Garcia-Gonzalez D, Jayamohan J, Sotiropoulos SN, Yoon SH, Cook J, Siviour CR, et al. On the mechanical behaviour of PEEK and HA cranial implants under impact loading. J Mech Behav Biomed Mater 2017;69:342–54. doi:10.1016/j.jmbbm.2017.01.012.
[26] Mutsaerts HJMM, van Dalen JW, Heijtel DFR, Groot PFC, Majoie CBLM, Petersen ET, et al. Cerebral perfusion measurements in elderly with hypertension using arterial spin labeling. PLOS ONE 2015;10:0133717. doi:10.1371/journal.pone.0133717.
[27] Heijtel DFR, Mutsaerts HJMM, Bakker E, Schober P, Stevens MF, Petersen ET, et al. Accuracy and precision of pseudo-continuous arterial spin labeling perfusion during baseline and hypercapnia: a head-to-head comparison with 15O $H_2O$ positron emission tomography. Neuroimage 2014;92:182–92. doi:10.1016/j.neuroimage.2014.02.011.
[28] Okell TW, Chappell MA, Kelly ME, Jezzard P. Cerebral blood flow quantification using vessel-encoded arterial spin labeling. J Cereb Blood Flow Metab 2013;33:1716–24. doi:10.1038/jcbfm.2013.129.
[29] Helthuis JHG, van Doormaal TPC, Hillen B, Bleys RLAW, Harteveld AA, Hendrikse J, et al. Branching pattern of the cerebral arterial tree. Anat Rec 2018:1–13. doi:10.1002/ar.23994.
[30] Karypis G, Kumar V. A fast and high quality multilevel scheme for partitioning irregular graphs. SIAM J Sci Comput 1998;20:359–92. doi:10.1137/S1064827595287997.
[31] Blinder P, Shih AY, Rafie C, Kleinfeld D. Topological basis for the robust distribution of blood to rodent neocortex. Proc Natl Acad Sci 2010;107:12670–5. doi:10.1073/pnas.1007239107.
[32] Schmid F, Barrett MJP, Jenny P, Weber B. Vascular density and distribution in neocortex. Neuroimage 2019;197:792–805. doi:10.1016/j.neuroimage.2017.06.046.
[33] Smith NP, Pullan AJ, Hunter PJ. An anatomically based model of transient coronary blood flow in the heart. SIAM J Appl Math 2002;62:990–1018.
[34] Boileau E, Nithiarasu P, Blanco PJ, Müller LO, Fossan FE, Hellevik LR, et al. A benchmark study of numerical schemes for one-dimensional arterial blood flow modelling. Int J Numer Method Biomed Eng 2015;31:02732. doi:10.1002/cnm.2732.
[35] Závodszky G, van Rooij B, Azizi V, Hoekstra A. Cellular level in-silico modeling of blood rheology with an improved material model for red blood cells. Front Physiol 2017;8:1–14. doi:10.3389/fphys.2017.00563.
[36] Olufsen MS. Structured tree outflow condition for blood flow in larger systemic arteries. Am J Physiol Circ Physiol 1999;276:H257–68. doi:10.1152/ajpheart.1999.276.1.H257.
[37] DeMers D, Wachs D. Physiology, Mean Arterial Pressure. StatPearls Publishing; 2019.
[38] Williams LR, Leggett RW. Reference values for resting blood flow to organs of man. Clin Phys Physiol Meas 1989;10:187–217. doi:10.1088/0143-0815/10/3/001.
[39] Fantini S, Sassaroli A, Tgavalekos KT, Kornbluth J. Cerebral blood flow and autoregulation: current measurement techniques and prospects for noninvasive optical methods. Neurophotonics 2016;3:031411. doi:10.1117/1.NPh.3.3.031411.
[40] Shapiro H, Stromberg D, Lee D, Wiederhielm C. Dynamic pressures in the pial arterial microcirculation. Am J Physiol Content 1971;221:279–83. doi:10.1152/ajplegacy.1971.221.1.279.
[41] Arrarte Terreros N, Tolhuisen ML, Bennink E, de Jong HWAM, Beenen LFM, Majoie CBLM, et al. From perviousness to permeability, modelling and measuring intra-thrombus flow in acute ischemic stroke. J Biomech 2020:110001. doi:10.1016/j.jbiomech.2020.110001.
[42] Ahn SH, D'Esterre CD, Qazi EM, Najm M, Rubiera M, Fainardi E, et al. Occult anterograde flow is an under-recognized but crucial predictor of early recanalization with intravenous tissue-type plasminogen activator. Stroke 2015;46:968–75. doi:10.1161/STROKEAHA.114.008648.
[43] Sorimachi T, Morita K, Ito Y, Fujii Y. Blood pressure measurement in the artery proximal and distal to an intra-arterial embolus during thrombolytic therapy. J Neurointerv Surg 2011;3:43–6. doi:10.1136/jnis.2010.003061.
[44] Duvernoy HM, Delon S, Vannson JL. Cortical blood vessels of the human brain. Brain Res Bull 1981;7:519–79. doi:10.1016/0361-9230(81)90007-1.
[45] Nishimura N, Schaffer CB, Friedman B, Lyden PD, Kleinfeld D. Penetrating arterioles are a bottleneck in the perfusion of neocortex. Proc Natl Acad Sci 2007;104:365–70. doi:10.1073/pnas.0609551104.
[46] Phan TG, Hilton J, Beare R, Srikanth V, Sinnott M. Computer modeling of anterior circulation stroke: proof of concept in cerebrovascular occlusion. Front Neurol 2014;5. doi:10.3389/fneur.2014.00176.
[47] Meng L, Gelb AW. Regulation of cerebral autoregulation by carbon dioxide. Anesthesiology 2015;122:196–205. doi:10.1097/ALN.0000000000000506.
[48] Payne S. Cerebral Autoregulation, s7-IV. Cham: Springer International Publishing; 2016. doi:10.1007/978-3-319-31784-7.
[49] Willie CK, Tzeng YC, Fisher JA, Ainslie PN. Integrative regulation of human brain blood flow. J Physiol 2014;592:841–59. doi:10.1113/jphysiol.2013.268953.
[50] Hall CN, Reynell C, Gesslein B, Hamilton NB, Mishra A, Sutherland BA, et al. Capillary pericytes regulate cerebral blood flow in health and disease. Nature 2014;508:55–60. doi:10.1038/nature13165.
[51] Copen WA, Schaefer PW, Wu O. MR Perfusion imaging in acute ischemic stroke. Neuroimaging Clin N Am 2011;21:259–83. doi:10.1016/j.nic.2011.02.007.